



## OPEN ACCESS

## EDITED BY

Xianguo Li,  
University of Waterloo, Canada

## REVIEWED BY

Pablo A. García-Salaberrí,  
Universidad Carlos III de Madrid, Spain  
Taikai Liu,  
Guangdong Academy of Sciences, China

## \*CORRESPONDENCE

Zhiming Bao,  
✉ zmbao@tju.edu.cn  
Bowen Qin,  
✉ qinbw@dfmc.com.cn

RECEIVED 24 June 2024

ACCEPTED 27 August 2024

PUBLISHED 11 September 2024

## CITATION

Qin Z, Liu Y, Tongsh C, Bao Z, Li H, Wu K,  
Deng Z, Qin B, Du Q and Jiao K (2024) *In-situ*  
visualization and structure optimization of the  
flow channel of proton exchange membrane  
fuel cells.

*Front. Energy Res.* 12:1454007.  
doi: 10.3389/fenrg.2024.1454007

## COPYRIGHT

© 2024 Qin, Liu, Tongsh, Bao, Li, Wu, Deng, Qin,  
Du and Jiao. This is an open-access article  
distributed under the terms of the [Creative  
Commons Attribution License \(CC BY\)](#). The use,  
distribution or reproduction in other forums is  
permitted, provided the original author(s) and  
the copyright owner(s) are credited and that the  
original publication in this journal is cited, in  
accordance with accepted academic practice.  
No use, distribution or reproduction is  
permitted which does not comply with these  
terms.

# *In-situ* visualization and structure optimization of the flow channel of proton exchange membrane fuel cells

Zhengguo Qin<sup>1</sup>, Yuanyuan Liu<sup>1</sup>, Chasen Tongsh<sup>1</sup>,  
Zhiming Bao<sup>1,2\*</sup>, Hongtao Li<sup>3</sup>, Kangcheng Wu<sup>3</sup>, Zhe Deng<sup>3</sup>,  
Bowen Qin<sup>3\*</sup>, Qing Du<sup>1</sup> and Kui Jiao<sup>1,2</sup>

<sup>1</sup>State Key Laboratory of Engines, Tianjin University, Tianjin, China, <sup>2</sup>National Industry-Education Platform for Energy Storage, Tianjin University, Tianjin, China, <sup>3</sup>Dongfeng Motor Corporation Research and Development Institute, Wuhan, China

The flow field serves as an important component of proton exchange membrane fuel cells (PEMFCs) for maintaining the hydration of the membrane and discharge of excessive water. In this study, a transparent polycarbonate plate was used as the cathode end plate of the PEMFC. The water management capacity of the PEMFCs with different cathode flow fields was evaluated. The movement and evolution patterns of water droplets, film, and columns in different flow fields were analyzed. The results show that liquid water is discharged faster as the cross-section of the flow channel becomes smaller. The performance of the PEMFC with a partially-narrowed flow field is higher due to better water management capacity and forced convection of gas reactant. Liquid water exists mostly in the form of liquid columns in the parallel flow channel, damaging the uniformity of gas distribution. The wavy flow field is likely to be flooded due to the difference of water movement velocity in different channel regions. In addition, a volume of fluid (VOF) model was developed to quantitatively evaluate the water management performance of each type of flow field. The water movement patterns in the different flow channels were concluded. This study provided real-time observations of water movement in the flow channel, revealing a correlation between water management capabilities and the performance of the PEMFC.

## KEYWORDS

PEMFC, optical visualization, water movement, transparent end plate, VOF model

## 1 Introduction

To reduce carbon emissions and environmental pollution caused by the extensive use of fossil fuels, the search for renewable and eco-friendly energy solutions has been an important issue worldwide (Jewell et al., 2018). Proton exchange membrane fuel cell (PEMFC) is considered one of the most promising energy transfer devices due to its high power density and zero emission (Jiao et al., 2021a; Parekh, 2022; Yao et al., 2024). Improving the water management capacity is one of the most important subjects among many engineering challenges for the PEMFC (Jiao et al., 2021b; Huo and Hall, 2023). A certain membrane hydration is required to promote effective ionic conductivity during the PEMFC operation. Too little water would dry the membrane out. Excessive accumulation of liquid water can lead to flooding, which induces localized hot spots and corrosion of cell components including electrodes, gas diffusion layer (GDL), etc. Then limited reactive gas

transport will negatively affect the performance, durability, and stability of PEMFCs (Min and Zhou, 2023; Wang et al., 2021; Nagulapati et al., 2023).

To improve the water management capacity of the cell, it is necessary to understand the liquid water movement within the flow field plates to achieve its structural optimization (Sun et al., 2023). According to research reports, the main techniques that can observe the water inside the fuel cell are neutron imaging technique (NIT) (Martinez et al., 2019; Manzi-Orezzoli et al., 2019), nuclear magnetic resonance imaging (NMR) (Mrad et al., 2023), X-ray radiography (XRR) (Kato et al., 2022; Tongsh et al., 2021; Martens et al., 2019), and optical visualization of PEMFCs (Rahimi-Esbo et al., 2017; Banerjee and Kandlikar, 2014), etc. The optical visualization technique uses hollowed-out flow field plates and transparent endplates to enable direct observation of liquid water within the flow channel. The method offers the advantage of high spatial and temporal resolution to capture the highly localized two-phase flow dynamics present in the channels, which has low operation cost and high convenience (Hu and Cao, 2016; Aslam et al., 2019). Zhan et al. (2012) applied the optical visualization technique and found that liquid water tends to accumulate in the region near the ridge due to flow rate difference and condensation of water vapor within the pores of GDL. At the same time, if the wall of the flow channel is more hydrophilic than the GDL surface, it tends to result in a liquid film covering the wall. Yin et al. (2022) achieved clear side imaging of water droplets in the flow channel of the PEMFC by using a high-speed camera. There are three stages of water droplet evolution. They are the growth stage, the oscillation stage, and the removal stage. The force balance of the water droplet in the three stages was revealed while the PEMFCs were operating. Rahimi-Esbo et al. (2020) designed a transparent PEMFC stack for investigating and evaluating the water management capacity when it operated at dead-end and open-end modes. An empirical correlation for estimating the required time for opening of purge valve was presented. Pei et al. (2022) obtained the liquid water distribution in the flow field through a transparent PEMFC. The liquid water formation characteristic was estimated according to the electric quantity produced. Based on transparent fuel cells segmented by printed circuit board, Meng et al. (2023) successfully revealed the correlation between cathode liquid water distribution and current density distribution in PEMFCs, which guides the flow field design and the development of water management strategies in fuel cell stacks. However, experimental observations are not able to obtain the details of interfacial changes. Therefore, many numerical simulation methods have also been applied in PEMFC flow channel research (Wang Y. et al., 2023; Zhao et al., 2023; Wang Z. et al., 2023). Among them, the volume of fluid (VOF) method has been widely used as a macroscopic interfacial capture method to study the two-phase flow characteristics in the flow channel. It was used to study the effects of the cross-section shapes of the PEMFC channel, the surface contact angles, the inlet velocities of air and water, as well as different droplet distributions on the water removal characteristics (Liao et al., 2022; Anyanwu et al., 2019; Chen et al., 2020). Dang and Zhou (2023) developed a three-dimensional VOF model to study the water removal process in cathode flow fields. They implemented a dynamic contact angle model to simulate the liquid behavior on GDLs. The observed liquid behavior agrees well with optical visualization results.

Above all, most of the studies focus on the liquid water movement in a single kind of flow field, but no comparisons

between different flow fields have been made. Some of the studies are based on offline devices. There is no consideration for the stochastic behavior of water generation in real fuel cells. In this study, an optical visualization fuel cell test system was designed and constructed to compare the water evolution patterns within different cathode flow fields during cell operation. The correspondence between the liquid water drainage in the flow field and the cell performance was analyzed by combining the polarization curve test and electrochemical impedance spectroscopy test (EIS). After that, based on the real-time observation results, an accurate VOF model was built to research the two-phase flow characteristics in the flow channel. The local optimization of the flow field structure was further discussed to provide an important theoretical reference for the improved water management capacity of PEMFCs.

## 2 Methodology

### 2.1 Experimental setup

A visualized cathode PEMFC was designed as shown in Figure 1A, the active area of the PEMFC in this study is 25 cm<sup>2</sup>. The membrane electrode assembly (MEA) is produced by Wuhan WUT HyPower Technology Co., Ltd., which includes a membrane of 8 μm, carbon papers of 167 μm, and catalytic layers (CLs) with 0.1 and 0.4 mg cm<sup>-2</sup> Pt loadings, corresponding to the anode and cathode, respectively. A heating pad is affixed to the anode plate for cell operating temperature control. The anode flow field plate is made of graphite with parallel flow fields cut on it. The visualized cathode consists of a hollowed-out flow field plate, a transparent plate, and a windowed end plate. The transparent plate is 8 mm thick, made of polycarbonate to prevent deformation during operating temperature, and is engraved with inlet and outlet air channels. The thickness of the hollowed-out flow field plate is equal to the height of the flow channel, which is 0.3 mm, and is made of stainless steel plated with gold (Dongguan SinoEtch Technology Co., Ltd.) to ensure electrical conductivity. The flow fields studied include parallel field, wavy flow field, and partially-narrowed flow field as shown in Figure 1C. The structural parameters of each flow field are shown in Table 1.

After the PEMFCs were assembled, the experiments were carried out by using a 400 W fuel cell test system (Ningbo Baite Testing Equipment Co., Ltd.), an electrochemical workstation (Zahner Zennium E), and a high-speed camera (Photron fastcam sa1.1) as shown in Figure 1B. A cold light source was chosen to avoid temperature interference during the shooting process. Performance analysis and real-time observation of liquid water can be performed in parallel. The specific operating conditions are shown in Table 2.

### 2.2 Numerical model

A VOF model was employed in the study to investigate the gas transport and liquid water dynamics in the different flow fields. Grid independence test and model validation have been conducted in our previous works (Bao et al., 2019; Bao et al., 2020). The model selected the two sides of the flow channel as the inlet and outlet, respectively. Figure 2 shows the computation domain for the straight flow channel, wavy channel, and partially-narrowed channel. The

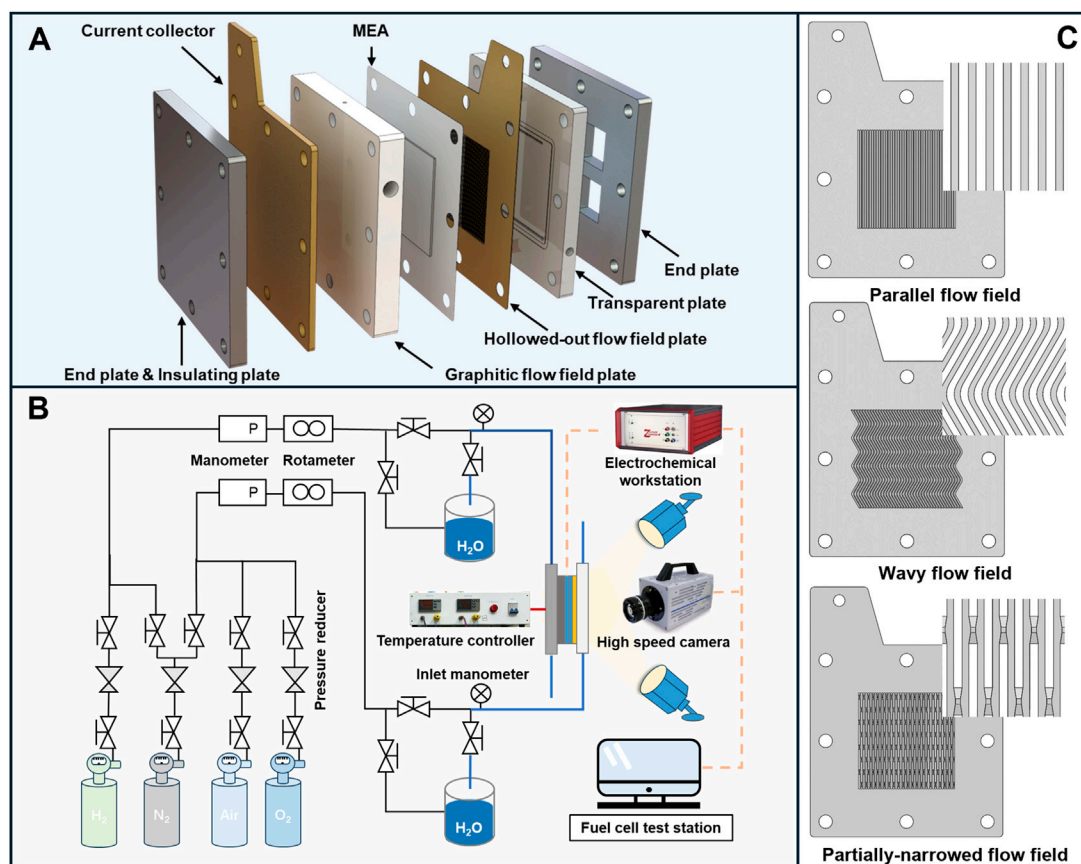


FIGURE 1 Assembly and testing of transparent PEMFCs: (A) Structure of cathode transparent fuel cell; (B) Schematic of the experimental system (Gong et al., 2023); (C) Cathode hollowed-out flow field plates.

TABLE 1 Structural parameters of different flow fields in the experimental PEMFC.

Parameter	Anode		Cathode (hollowed-out)	
	Parallel flow field	Parallel flow field	Wavy flow field	Partially-narrowed flow field
Number of channels	42	42	39	42
Number of lands	41	41	38	41
Width of channels (W) (mm)	0.67	0.67	0.67	0.67
Height of channels (H) (mm)	0.3	0.3	0.3	0.3
Width of lands (mm)	0.53	0.53	0.53	0.53
Wave amplitude (A) (mm)	—	—	1.76	—
Wave period (T) (mm)	—	—	14.34	—
Length of narrowed region ( $I_1$ ) (mm)	—	—	—	2.5
Interval of narrowed region ( $I_2$ ) (mm)	—	—	—	13
Length of the neck of narrowed region ( $I_3$ ) (mm)	—	—	—	0.5
Width of the neck of narrowed region (w) (mm)	—	—	—	0.4
Height of the neck of narrowed region (h) (mm)	—	—	—	0.2

TABLE 2 Operating conditions of the PEMFCs.

Operating condition	Anode	Cathode (hollowed-out)
Reactant type	Hydrogen	Oxygen
Operating temperature	80°C	80°C
Back pressure	0 kPa	0 kPa
Relative humidity (RH)	100%	100%
Stoichiometric ratio (ST)	1.5	2.0

TABLE 3 Initial and boundary conditions for the cases in this study.

Parameter	Value
Gas inlet velocity (m s <sup>-1</sup> )	3.3
Length of the channel (mm)	56
liquid volume (mL)	0.000135
Back pressure (atm)	1
The static contact angle of the GDL surface (°)	138
The static contact angles of the channel walls (°)	102

initial and boundary conditions of cases are listed in Table 3. The liquid is initialized in the form of a droplet near the inlet of the flow channel. The inlet velocity is given as 3.3 m s<sup>-1</sup>, approximately equalling to the gas velocity in the operating PEMFC under 1.2 A cm<sup>-2</sup>. Total pressure (1 atm) is defined at the outlet and non-slip boundary is set for all the walls. The static contact angles of surfaces set in the model are derived from the averaged values measured at different places, as shown in Figure 3.

The VOF method represents local phase change in the computational domain by defining phase volume fraction and realizes the capture of the phase interface by solving the phase volume fraction equation. The governing equations of the VOF method are as follows (Hirt and Nichols, 1981; Pilliod and Puckett, 2004):

$$\nabla \cdot \vec{U} = 0$$

$$\frac{\partial \alpha}{\partial t} + \nabla \cdot (\vec{U}\alpha) + \nabla \cdot [\vec{U}_r \alpha (1 - \alpha)] = 0$$

$$\frac{\partial(\rho \vec{U})}{\partial t} + \nabla \cdot (\rho \vec{U} \vec{U}) + = \nabla \cdot (2\mu D) - \nabla p_d - \vec{g} \cdot \vec{y} \nabla \rho + \sigma \kappa \nabla \alpha$$

where  $\vec{U}$  is the velocity vector of each phase fluid,  $\vec{U}_r$  is the compression velocity, defined as the relative velocity at the gas-liquid interface.  $\alpha$  is defined as the phase volume fraction in each control volume.  $\alpha = 0$  means that the fluid in the control volume is gas,  $\alpha = 1$  means that the control volume is full of liquid, and  $0 < \alpha <$

1 means that there is a phase interface in control volume.  $\sigma$  and  $\kappa$  are the surface tension coefficient and average interface curvature, respectively.  $D$  is the deformation rate tensor with the expression  $[\nabla \vec{U} + (\nabla \vec{U})^T]/2$ .  $\rho$  and  $\mu$  are the density (kg/m<sup>3</sup>) and dynamic viscosity (kg/(m·s)). Based on the phase volume fraction  $\alpha$ , the density and viscosity of the fluid are re-expressed as:

$$\rho = \rho_l \alpha + \rho_g (1 - \alpha)$$

$$\mu = \mu_l \alpha + \mu_g (1 - \alpha)$$

where the subscripts l and g denote the liquid and gas phases, respectively.

The boundary conditions are simplified by defining the modified pressure  $p_d$ :

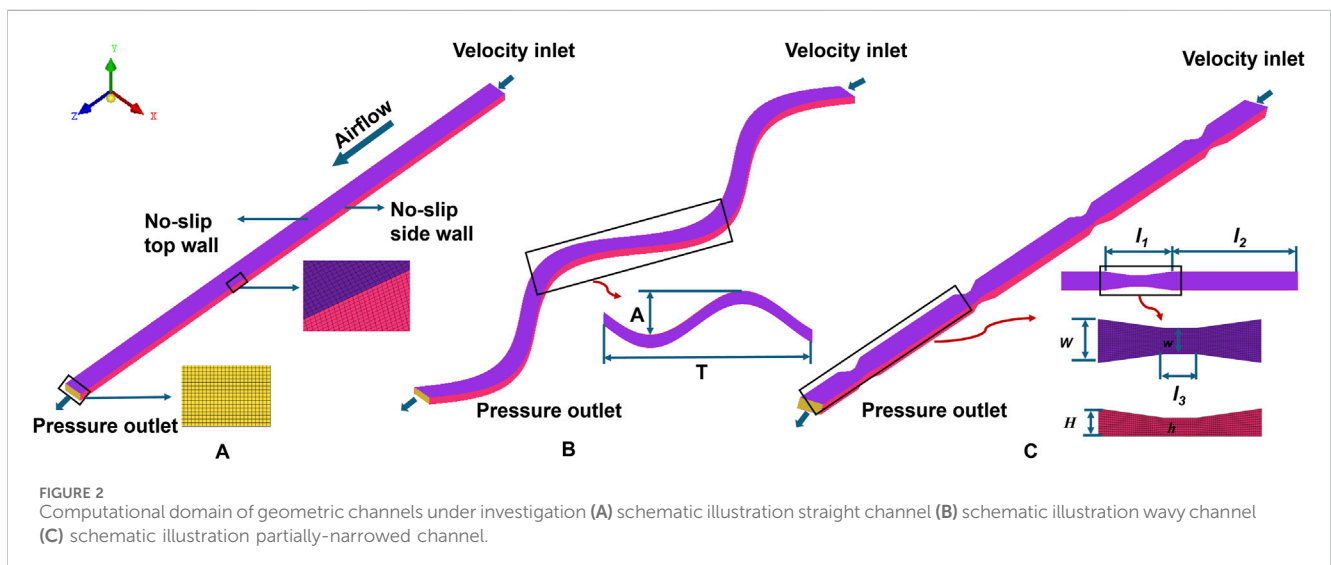
$$p_d = p - \rho \vec{g} \cdot \vec{y}$$

where  $\vec{y}$  is the position vector.

### 3 Results and discussion

#### 3.1 In-situ optical visualization of liquid water in flow fields

After the activation process in constant potential mode, the PEMFCs assembled with different flow fields were tested separately.



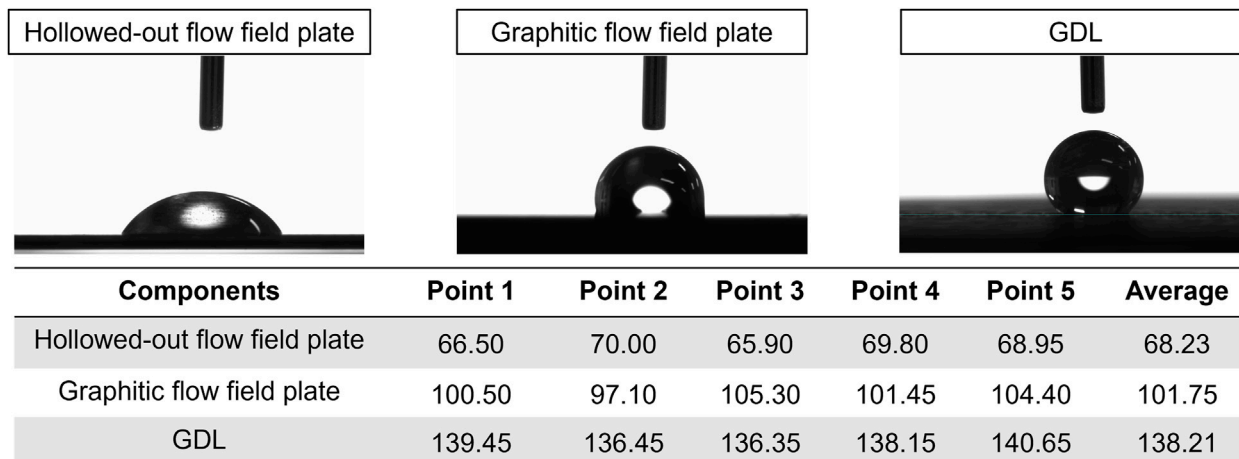


FIGURE 3 The static contact angles of surfaces for different components in the PEMFC.

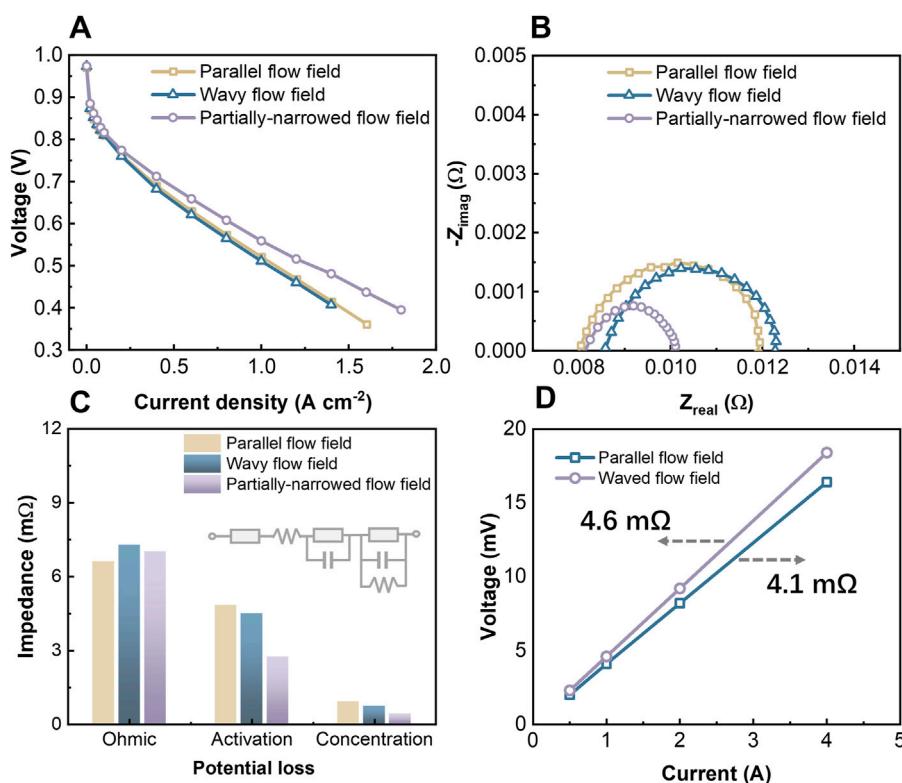
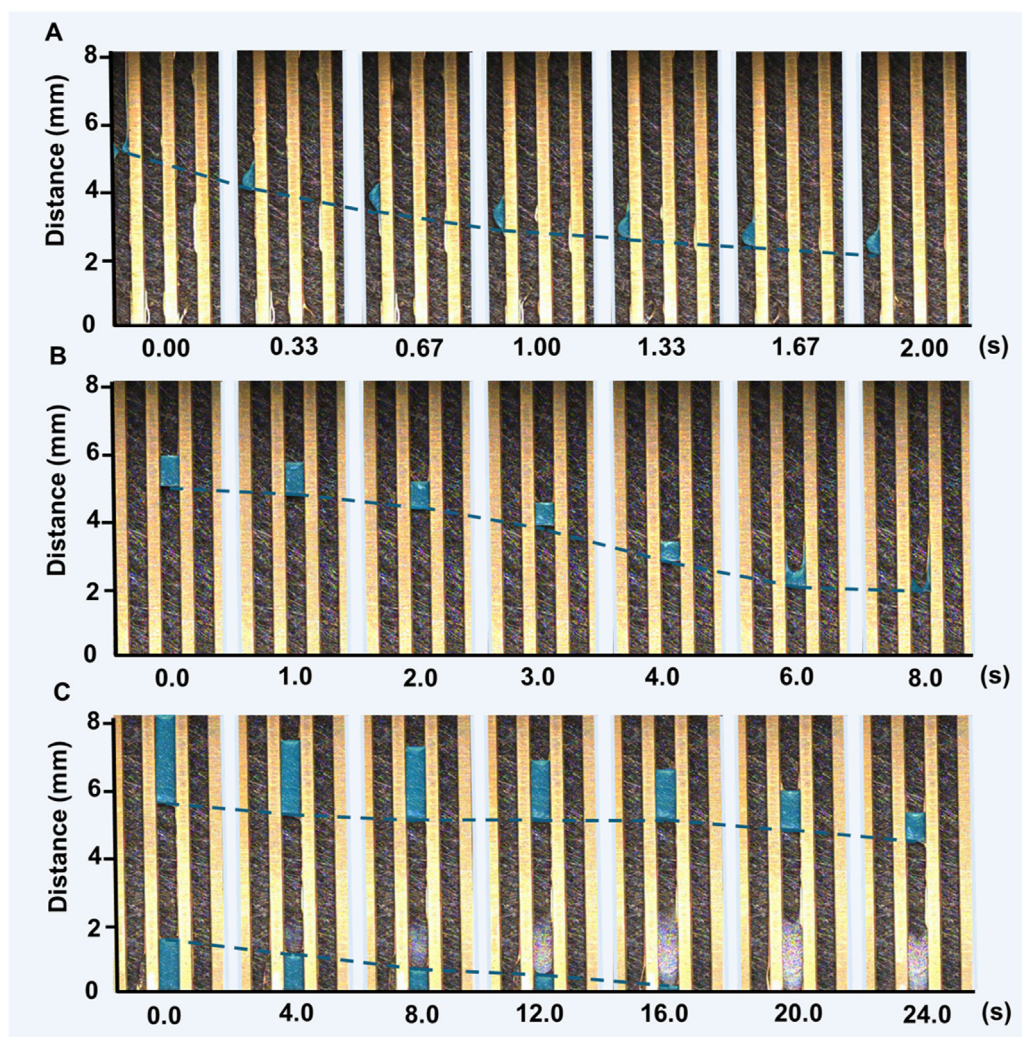


FIGURE 4 Experimental comparison of PEMFCs with different cathode flow fields: (A) Polarization curves; (B) EIS test results and (C) equivalent circuit (Tongsh et al., 2024) fitting results under 1.2 A cm<sup>-2</sup>; (D) The electrical contact resistance difference between GDLs and hollowed-out flow field plates.

According to Figure 4A, it is found that the parallel flow field and the wavy flow field have similar performance, while the partially-narrowed flow field shows the highest performance among the three, even in high current densities. It shows better water management capacity and efficient mass transfer. As shown in Figures 4B, C, the ohmic impedance of the PEMFC assembled with a partially-narrowed flow field is higher than the one with the parallel flow field, but the mass

transfer and activation losses are reduced. The periodic narrowed channels in the partially-narrowed flow field lead to an enhanced gas mass transfer in the through-plane direction while the gas flow rate is also increased. However, the high gas flow rate reduces the hydration of the membrane compared with the parallel flow field. The wavy flow field has higher ohmic losses than the parallel flow field due to the bigger hollowed-out region, which causes larger electron transport



**FIGURE 5** Real-time observations of liquid water movement in the parallel flow field: (A) Movement of droplets; (B) Movement of a liquid column; (C) Movement of multiple liquid columns in a single flow channel.

resistance. It is proved by the I-V test in the [Figure 4D](#). The test was conducted by replacing the MEA with a carbon paper to focus on the difference in contact resistance between the hollowed-out flow field plates and GDLs. However, the periodic change of gas flow direction increases the mass transfer to the GDL. The mass transfer and activation losses are reduced, resulting in the cell performance similar to that with the parallel flow field.

The comparison of different flow fields on real-time observation results is consistent with the performance comparison. As shown in [Figure 5](#), there is water accumulating in the flow channels of the parallel flow field, mostly in the form of liquid columns and liquid droplets. The liquid droplets move much faster than the liquid column. Because the gas tends to flow through the flow channel with less flow resistance. Once there is a channel blocked by liquid columns, the gas flow flux will be reduced, and the liquid column removal speed will be reduced as well. The phenomena lead to uneven distribution of the reactants in the flow channel. Fortunately, the pressure difference between the inlet and outlet of the channels always exists. The liquid column can still move slowly

by the force. The moving speed of liquid columns is lower and lower with the number of water increasing in a channel as shown in [Figure 5C](#). Specifically, the liquid column size will gradually decrease with the gas blowing. Then the column discharges or breaks up when the liquid column size is small enough. This is because water is constantly sticking to the walls in the form of film as it flows through channels due to the hydrophilicity of the channel walls, which is proved in [Figure 3](#). Besides, confined chambers are formed between the liquid columns when multiple liquid columns are present in a flow channel. The heat generated in the active region surrounded by the liquid columns and walls is not easily carried away, which increases the possibility of causing localized hot spots.

For the wavy flow field, although the periodic change of gas flow direction can improve the water removal capacity, which is proved by the EIS test result in [Figure 4B](#), there is still water accumulation in the channels as shown in [Figure 6A](#). An interesting phenomenon was discovered. The droplets move faster when they pass through non-bending regions than bending regions. In this case, the retention of droplets in the bend region is likely to cause the

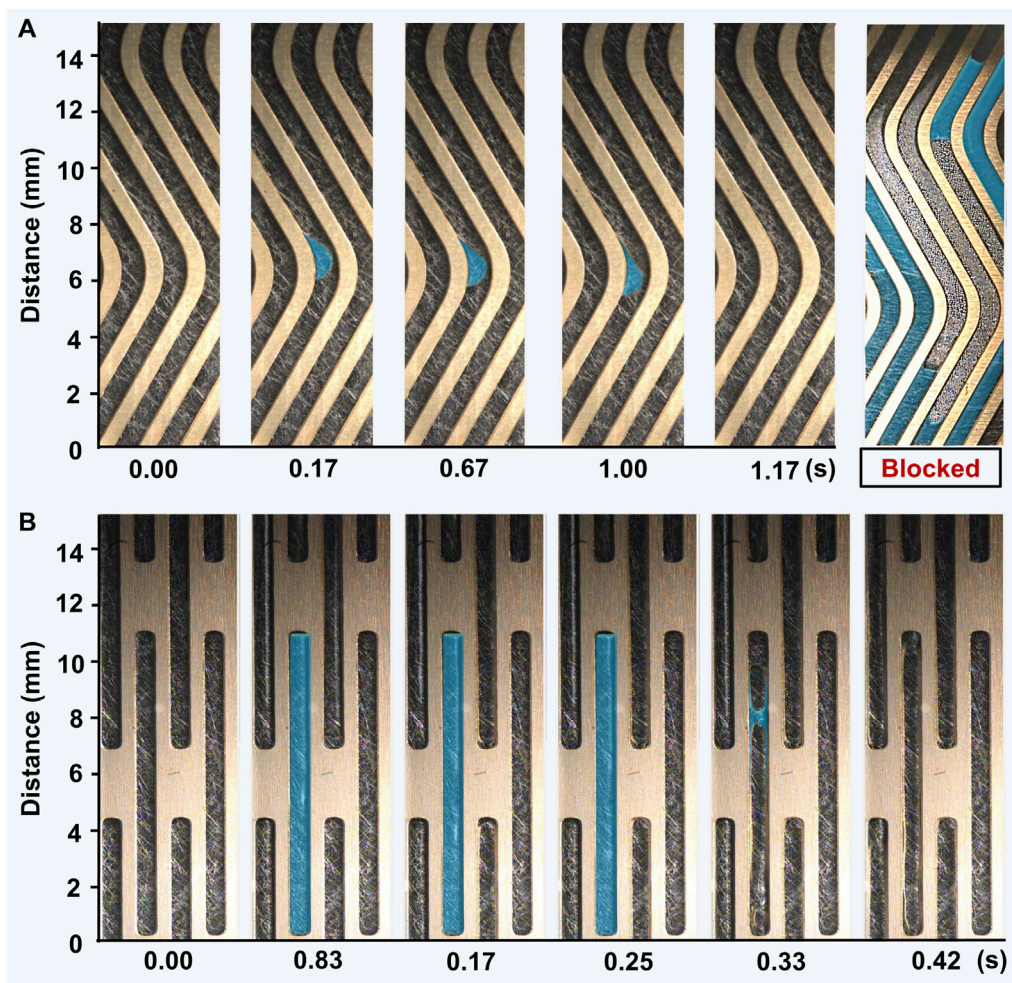


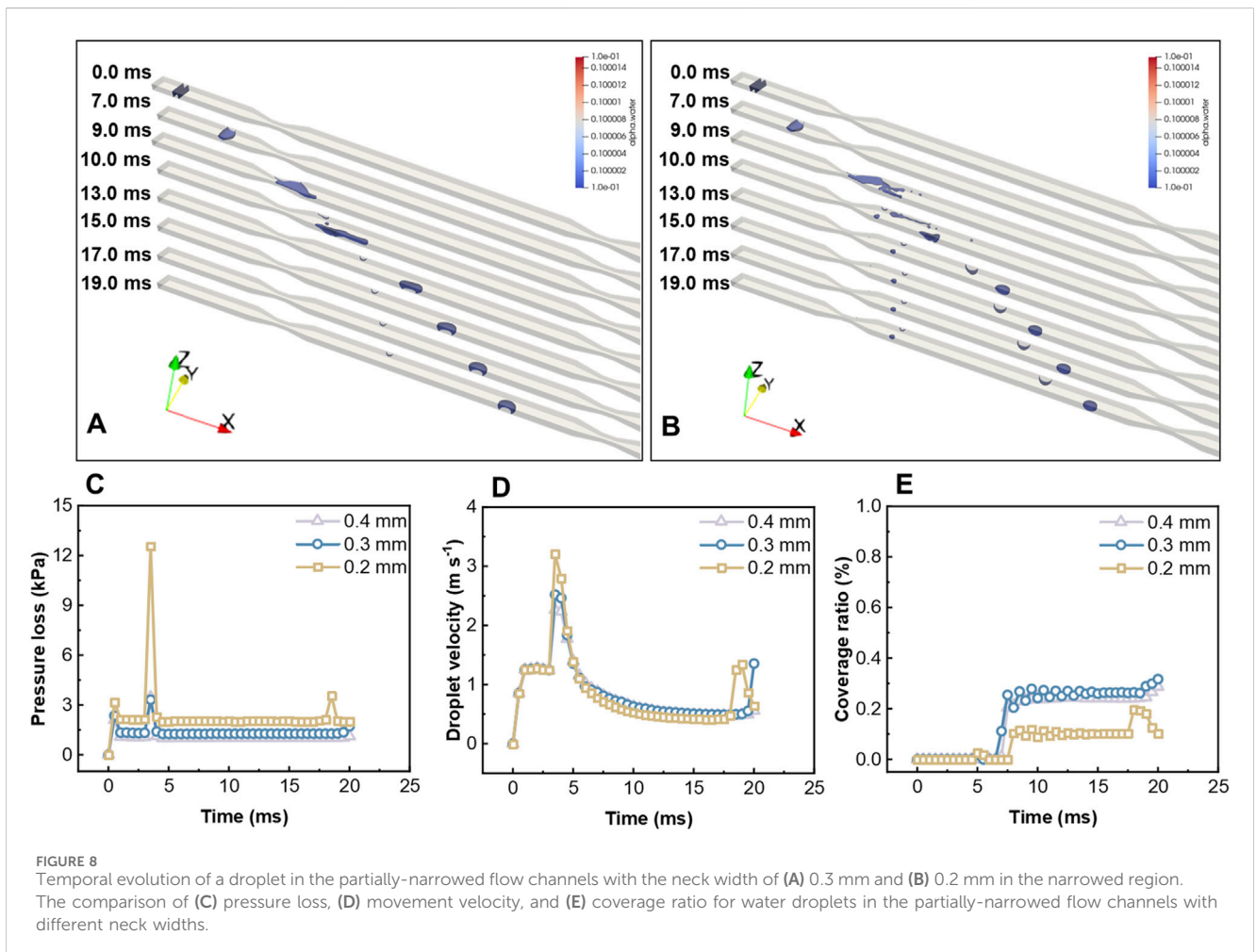
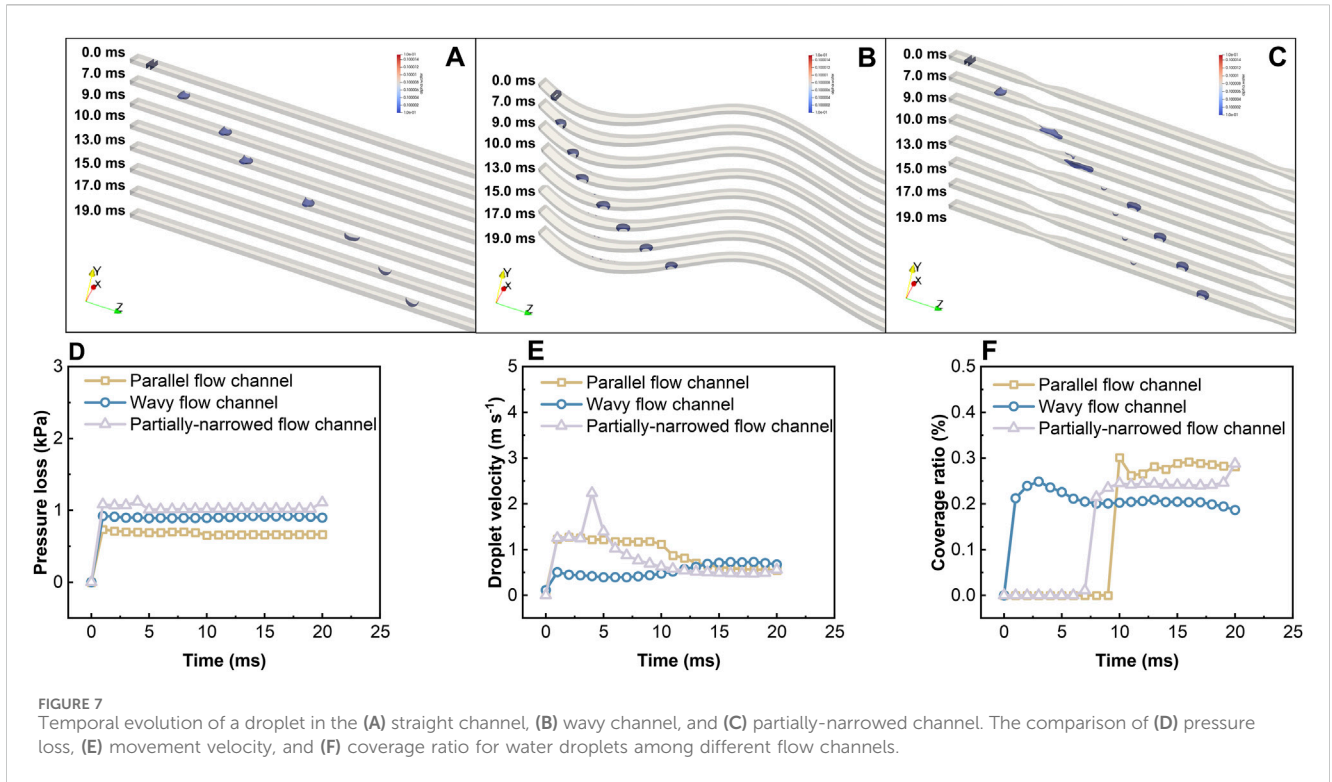
**FIGURE 6**  
Real-time observations of liquid water movement in the different flow fields: (A) Velocity differences of liquid droplets through different regions of the wavy flow channel; (B) Rapid movement of liquid water in the partially-narrowed flow field.

accumulation of liquid water, which in turn leads to the restriction of the reactant transfer efficiency. However, the partially-narrowed flow field shows excellent drainage ability. As shown in Figure 6B, the periodic change of the cross-sectional area of the partially-narrowed channel increases the gas flow rate significantly. The liquid water removal velocity in partially-narrowed flow fields is significantly higher than that in parallel flow fields. Although the membrane hydration is lower, the gas transfer in the through-plane direction is enhanced. This is reflected in the EIS test results as shown in Figure 4B. Therefore, the partially-narrowed flow field is conducive to the transmission of gas to the electrode reaction interface, improving the utilization rate of reactants and discharging the products in time. It has excellent performance.

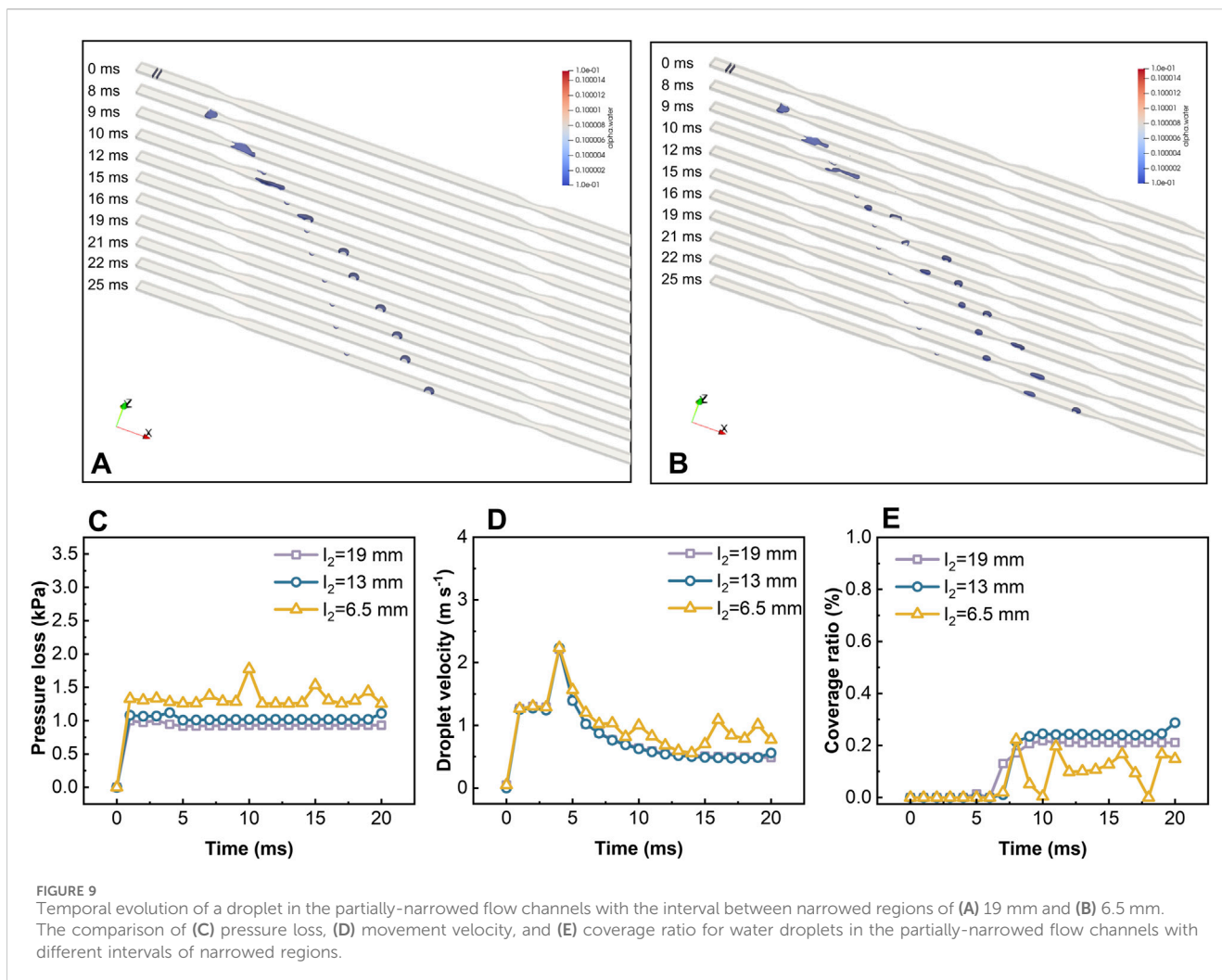
### 3.2 Model analysis of liquid behaviors in a single flow channel

To quantitatively evaluate the water management performance of each type of flow field, this section investigated the water removal process of a single droplet in a single flow channel regarding liquid

behaviors, pressure drop, coverage ratio, and droplet velocity. As shown in Figures 7A–C, we placed the same droplet at the inlet of different flow channels. It was found that the gas flow resistance is increased when a wavy or partially-narrowed channel is placed in the flow field as shown in Figure 7D. For a straight channel, the droplet moves fast in the channel if there is no water blockage happening. Liquid water tends to adhere on the side walls of channels under gas flow. In contrast, for a wavy channel, the contact of water with the GDL surface is reduced due to centrifugal force and adsorption on the hydrophilic wall when a droplet passes through the bending region, then the coverage ratio is low as shown in Figure 7E. The droplet moves slower in the wavy flow field due to the change in flow direction as shown in Figure 7F. The droplet shows an increase in velocity as they pass through each neck in the partially-narrowed flow channel, along with break-up into small droplets, which is consistent with experimental observation. Although the coverage ratio is slightly larger, it shows superior water removal capacity because of increased gas flow rate by narrowed regions. This can prevent the accumulation of droplets and improve the mass transfer efficiency of the reactants.





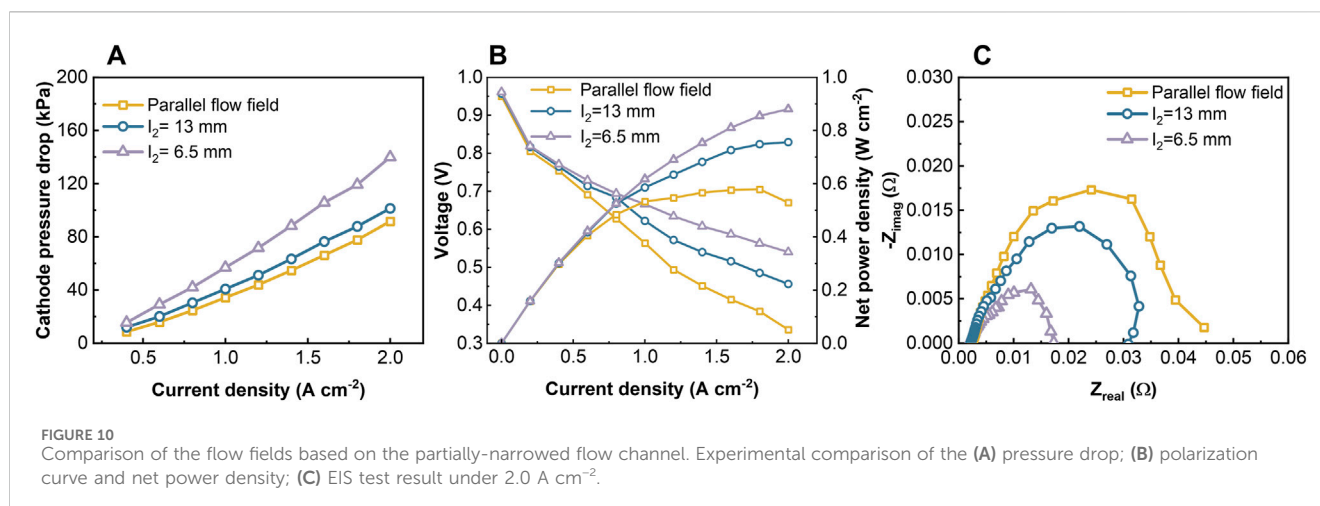


### 3.3 Optimization of the partially-narrowed flow channel

To further optimize the water management capacity of the partially-narrowed flow channel. The width of neck of the partially-narrowed channel were reduced from 0.4 to 0.3, 0.2 mm. The observed moving behavior of liquid water in the channels is shown in [Figures 8A, B](#). The flow resistance and the water droplet moving velocity will increase with the neck width decrease, which is shown in [Figures 8C–E](#). Correspondingly, the breakup of liquid droplets is more significant. When the neck width is 0.2 mm, the surface coverage of droplets in the GDL is extremely small, which means that liquid water can be discharged efficiently in the form of small droplets. Reducing cross-section area of the neck or increasing the number of narrowed parts will help discharging water from the fuel cell. However, the excessive pressure loss in the flow channel will reduce the net power output. The flow rate connects the hydration of membrane. Therefore, it is necessary to arrange the neck area and number according to the actual operating conditions of the fuel cell.

As shown in the [Figures 9A, B](#), for a partially-narrowed flow channel, each narrowed region in the flow channel could induce

droplet break-up. In this study, the interval length between narrowed regions in the partially-narrowed flow channel is denoted by  $I_2$ . There is no clear difference in droplet behavior when  $I_2$  is 19 or 13 mm. As shown in the [Figures 9C–E](#), when  $I_2$  is reduced to 6.5 mm, a slight increase in the pressure drop in the flow channel occurs. The movement velocity and the surface coverage in the GDL of droplets show large fluctuations. Specifically, the fluctuations of the coverage ratio are between 0.2% and 0, which indicates that decreasing the interval between narrowed regions is favorable for the removal of liquid water. Compared to reducing the width of the neck, this option can achieve liquid water removal with a slight increase in pressure loss, which is a more effective. As shown in [Figure 10](#), the partially-narrowed flow channel with different interval lengths of narrowed regions was applied to the cathode flow field to assemble a conventional fuel cell with 25 cm<sup>2</sup> active area. It was found that a performance enhancement in line with expectations occurred. Compared to the parallel flow field, the net power density of the PEMFC assembling partially-narrowed flow field with  $I_2$  of 13 mm as well as 6.5 mm is increased by 22% and 43% under the voltage of 0.65 V, respectively ([Nathaniel et al., 2016](#)). At high current densities, partially-narrowed flow fields show good drainage capacity, which ensures the efficiency of the reactive gas transport and reduces the concentration and activation losses.



## 4 Conclusion

Water management capacity is essential for the performance and stable operation of PEMFCs. This study used an optical visualization method to achieve real-time observation of liquid water inside different cathode flow fields during cell operation. The behaviors of liquid water in different flow fields were studied. A VOF model was built to quantify the liquid removal performance of different channels. The main conclusions are as follows:

1. Compared with the parallel flow field, the mass transfer loss of the PEMFCs with wavy flow field and partially-narrowed flow field is lower. The reason is that the gas flow direction changes periodically, which enhances both reactant distribution and through-plane convection. Specifically, the gas flow rate and pressure are periodically changed in the partially-narrowed flow field, which promotes the under-rib cross flow with MEA.
2. In the wavy flow field, the liquid water is removed more slowly but covers a smaller area of GDL surface than the parallel flow field because the inertia effect induced by the periodically changed gas flow direction enhances the adhesion effect of side walls. A lower coverage area of GDL surface indicates a higher mass transfer efficiency between flow field and GDL.
3. In the partially-narrowed flow field, periodically changed gas flow rate promotes both the discharge and the breakup of liquid droplets/columns at the necks of narrowed zones. But membrane hydration could be reduced by the increased pressure drop and through-plane convection. Therefore, the area of the necks and interval length between narrowed regions of the partially-narrowed flow field should be designed considering the change of ohmic loss and pumping loss.

## Data availability statement

The original contributions presented in the study are included in the article/supplementary material, further inquiries can be directed to the corresponding authors.

## Author contributions

ZQ: Conceptualization, Methodology, Validation, Writing–original draft. YL: Methodology, Software, Writing–original draft. CT: Data curation, Methodology, Writing–original draft. ZB: Funding acquisition, Methodology, Supervision, Writing–review and editing. HL: Project administration, Writing–original draft, Supervision. KW: Project administration, Writing–original draft, Methodology. ZD: Project administration, Writing–original draft. BQ: Methodology, Project administration, Supervision, Writing–original draft. QD: Funding acquisition, Resources, Writing–review and editing. KJ: Funding acquisition, Resources, Writing–review and editing, Methodology, Supervision.

## Funding

The author(s) declare that financial support was received for the research, authorship, and/or publication of this article. This research is supported by the National Key Research and Development Program of China (Grant No. 2023YFB4005800), and the China National Postdoctoral Program for Innovative Talent (Grant No. BX20230258).

## Conflict of interest

Authors HL, KW, ZD and BQ were employed by company Dongfeng Motor Corporation Research and Development Institute.

The remaining authors declare that the research was conducted in the absence of any commercial or financial relationships that could be construed as a potential conflict of interest.

The author(s) declared that they were an editorial board member of Frontiers, at the time of submission. This had no impact on the peer review process and the final decision.

## Publisher's note

All claims expressed in this article are solely those of the authors and do not necessarily represent those of their affiliated

organizations, or those of the publisher, the editors and the reviewers. Any product that may be evaluated in this article, or

claim that may be made by its manufacturer, is not guaranteed or endorsed by the publisher.

## References

- Anyanwu, I. S., Hou, Y., Xi, F., Wang, X., Yin, Y., Du, Q., et al. (2019). Comparative analysis of two-phase flow in sinusoidal channel of different geometric configurations with application to PEMFC. *Int. J. Hydrog. Energy* 44, 13807–13819. doi:10.1016/j.ijhydene.2019.03.213
- Aslam, R. M., Ingham, D. B., Ismail, M. S., Hughes, K., and Pourkashanian, M. (2019). Simultaneous thermal and visual imaging of liquid water of the PEM fuel cell flow channels. *J. Energy Inst.* 92, 311–318. doi:10.1016/j.joeci.2018.01.005
- Banerjee, R., and Kandlikar, S. G. (2014). Liquid water quantification in the cathode side gas channels of a proton exchange membrane fuel cell through two-phase flow visualization. *J. Power Sources* 247, 9–19. doi:10.1016/j.jpowsour.2013.08.016
- Bao, Z., Niu, Z., and Jiao, K. (2019). Numerical simulation for metal foam two-phase flow field of proton exchange membrane fuel cell. *Int. J. Hydrog. Energy* 44 (12), 6229–6244. doi:10.1016/j.ijhydene.2019.01.086
- Bao, Z., Wang, Y., and Jiao, K. (2020). Liquid droplet detachment and dispersion in metal foam flow field of polymer electrolyte membrane fuel cell. *J. Power Sources* 480, 229150. doi:10.1016/j.jpowsour.2020.229150
- Chen, R., Qin, Y., Ma, S., and Du, Q. (2020). Numerical simulation of liquid water emerging and transport in the flow channel of PEMFC using the volume of fluid method. *Int. J. Hydrog. Energy* 45, 29861–29873. doi:10.1016/j.ijhydene.2019.07.169
- Dang, D. K., and Zhou, B. (2023). Effects of pin shapes on gas-liquid transport behaviors in PEMFC cathode. *J. Power Sources* 557, 232584. doi:10.1016/j.jpowsour.2022.232584
- Gong, Z., Wang, B., Xing, Y., Xu, Y., Qin, Z., Chen, Y., et al. (2023). High-precision and efficiency diagnosis for polymer electrolyte membrane fuel cell based on physical mechanism and deep learning. *eTransportation* 18, 100275. doi:10.1016/j.etrans.2023.100275
- Hirt, C. W., and Nichols, B. D. (1981). Volume of fluid (VOF) method for the dynamics of free boundaries. *J. Comput. Phys.* 39 (1), 201–225. doi:10.1016/0021-9991(81)90145-5
- Hu, M., and Cao, G. (2016). Research on the performance differences between a standard PEMFC single cell and transparent PEMFC single cells using optimized transparent flow field unit—Part I: design optimization of a transparent flow field unit. *Int. J. Hydrog. Energy* 41, 2955–2966. doi:10.1016/j.ijhydene.2015.12.144
- Huo, D., and Hall, C. (2023). Data-driven prediction of temperature variations in an open cathode proton exchange membrane fuel cell stack using Koopman operator. *Energy AI* 14, 100289. doi:10.1016/j.egyai.2023.100289
- Jewell, J., McCollum, D., Emmerling, J., Bertram, C., Gernaat, D. E. H. J., Krey, V., et al. (2018). Limited emission reductions from fuel subsidy removal except in energy-exporting regions. *Nature* 554, 229–233. doi:10.1038/nature25467
- Jiao, K., Wang, B., Du, Q., Wang, Y., Zhang, G., Yang, Z., et al. (2021b). Water and thermal management of proton exchange membrane fuel cells. *Elsevier*. doi:10.1016/B978-0-323-91116-0.00001-8
- Jiao, K., Xuan, J., Du, Q., Bao, Z., Xie, B., Wang, B., et al. (2021a). Designing the next generation of proton-exchange membrane fuel cells. *Nature* 595 (7867), 361–369. doi:10.1038/s41586-021-03482-7
- Kato, A., Kato, S., Yamaguchi, S., Suzuki, T., and Nagai, Y. (2022). Mechanistic insights into water transport in polymer electrolyte fuel cells with a variation of cell temperature and relative humidity of inlet gas elucidated by operando synchrotron X-ray radiography. *J. Power Sources* 521, 230951. doi:10.1016/j.jpowsour.2021.230951
- Liao, J., Yang, G., Li, S., Shen, Q., Jiang, Z., Wang, H., et al. (2022). Study of droplet flow characteristics on a wetting gradient surface in a proton exchange membrane fuel cell channel using lattice Boltzmann method. *J. Power Sources* 529, 231245. doi:10.1016/j.jpowsour.2022.231245
- Manzi-Orezzi, V., Mularczyk, A., Trtik, P., Halter, J., Eller, J., Schmidt, T. J., et al. (2019). Coating distribution analysis on gas diffusion layers for polymer electrolyte fuel cells by neutron and X-ray high-resolution tomography. *ACS Omega* 4, 17236–17243. doi:10.1021/acsomega.9b01763
- Martens, I., Vamvakeros, A., Chattot, R., Blanco, M. V., Rasola, M., Pusa, J., et al. (2019). X-ray transparent proton-exchange membrane fuel cell design for *in situ* wide and small angle scattering tomography. *J. Power Sources* 437, 226906. doi:10.1016/j.jpowsour.2019.226906
- Martinez, N., Porcar, L., Escribano, S., Micoud, F., Rosini, S., Tengattini, A., et al. (2019). Combined operando high resolution SANS and neutron imaging reveals *in-situ* local water distribution in an operating fuel cell. *ACS Appl. Energy Mater.* 2, 8425–8433. doi:10.1021/acsaem.9b01266
- Meng, K., Zhou, H., Yang, G., Chen, W., and Chen, B. (2023). Local performance response behavior during liquid water transport of a hydrogen–oxygen proton exchange membrane fuel cell: an experimental investigation. *Energy Conv. Manag.* 293, 117510. doi:10.1016/j.enconman.2023.117510
- Min, T., and Zhou, Q. (2023). Effects of liquid water on transport in the catalyst layer of proton exchange membrane fuel cells. *Front. Energy Res.* 11, 1330124. doi:10.3389/fenrg.2023.1330124
- Mrad, C., Perrin, J., Kaddouri, A. E., Guendouz, L., Mozet, K., Dillet, J., et al. (2023). NMR characterization of proton exchange membranes in controlled hygrometry conditions. *J. Membr. Sci.* 688, 122111. doi:10.1016/j.memsci.2023.122111
- Nagulapati, V., Shiva Kumar, S., Annadurai, V., and Lim, H. (2023). Machine learning based fault detection and state of health estimation of proton exchange membrane fuel cells. *Energy AI* 12, 100237. doi:10.1016/j.egyai.2023.100237
- Nathaniel, J. C., Travis, S., Anthony, D. S., and Park, J. W. (2016). Experimental optimization of parallel and interdigitated PEMFC flow-field channel geometry. *Int. J. Hydrog. Energy* 41 (2), 1213–1223. doi:10.1016/j.ijhydene.2015.11.153
- Parekh, A. (2022). Recent developments of proton exchange membranes for PEMFC: a review. *Front. Energy Res.* 10, 956132. doi:10.3389/fenrg.2022.956132
- Pei, H., Xiao, C., and Tu, Z. (2022). Experimental study on liquid water formation characteristics in a novel transparent proton exchange membrane fuel cell. *Appl. Energy* 321, 119349. doi:10.1016/j.apenergy.2022.119349
- Pilliod, J. D., and Puckett, E. D. (2004). Second-order accurate volume-of-fluid algorithms for tracking material interfaces. *J. Comput. Phys.* 199 (2), 465–502. doi:10.1016/j.jcp.2003.12.023
- Rahimi-Esbo, M., Ramiar, A., Ranjbar, A. A., and Alizadeh, E. (2017). Design, manufacturing, assembling and testing of a transparent PEM fuel cell for investigation of water management and contact resistance at dead-end mode. *Int. J. Hydrog. Energy* 42, 11673–11688. doi:10.1016/j.ijhydene.2017.02.030
- Rahimi-Esbo, M., Ranjbar, A. A., and Rahgoshay, S. M. (2020). Analysis of water management in PEM fuel cell stack at dead-end mode using direct visualization. *Renew. Energy* 162, 212–221. doi:10.1016/j.renene.2020.06.078
- Sun, F., Su, D., Li, P., and Dong, X. (2023). A novel 3D fine-mesh flow field design and performance analysis for proton exchange membrane fuel cells. *J. Power Sources* 584, 233572. doi:10.1016/j.jpowsour.2023.233572
- Tongsh, C., Liang, Y., Xie, X., Li, L., Liu, Z., Du, Q., et al. (2021). Experimental investigation of liquid water in flow field of proton exchange membrane fuel cell by combining X-ray with EIS technologies. *Sci. China Technol. Sci.* 64, 2153–2165. doi:10.1007/s11431-021-1815-6
- Tongsh, C., Wu, S., Jiao, K., Huo, W., Du, Q., Park, J. W., et al. (2024). Fuel cell stack redesign and component integration radically increase power density. *Joule* 8 (1), 175–192. doi:10.1016/j.joule.2023.12.003
- Wang, X. R., Ma, Y., Gao, J., Li, T., Jiang, G., and Sun, Z. (2021). Review on water management methods for proton exchange membrane fuel cells. *Int. J. Hydrog. Energy* 46, 12206–12229. doi:10.1016/j.ijhydene.2020.06.211
- Wang, Y., Wu, K., Zhao, H., Li, J., Sheng, X., Yin, Y., et al. (2023). Degradation prediction of proton exchange membrane fuel cell stack using semi-empirical and data-driven methods. *Energy AI* 11, 100205. doi:10.1016/j.egyai.2022.100205
- Wang, Z., Liu, Z., Fan, L., Du, Q., and Jiao, K. (2023). Application progress of small-scale proton exchange membrane fuel cell. *Energy Rev.* 2, 100017. doi:10.1016/j.enrev.2023.100017
- Yao, J., Wu, Z., Wang, B., Yang, Y., Yang, F., Zhang, Z., et al. (2024). High-stability dead-end anode proton exchange membrane fuel cells by purge optimization. *J. Power Sources* 595, 234062. doi:10.1016/j.jpowsour.2024.234062
- Yin, Y., Li, Y., Qin, Y., Li, M., Liu, G., Zhang, J., et al. (2022). *Ex-situ* experimental study on dynamic behaviors and detachment characteristics of liquid water in a transparent channel of PEMFC. *Renew. Energy* 187, 1037–1049. doi:10.1016/j.renene.2022.02.031
- Zhan, Z., Wang, C., Fu, W., and Pan, M. (2012). Visualization of water transport in a transparent PEMFC. *Int. J. Hydrog. Energy* 37, 1094–1105. doi:10.1016/j.ijhydene.2011.02.081
- Zhao, C., Yuan, S., Cheng, X., Zheng, Z., Liu, J., Yin, J., et al. (2023). The effect of catalyst layer design on catalyst utilization in PEMFC studied via stochastic reconstruction method. *Energy AI* 13, 100245. doi:10.1016/j.egyai.2023.100245